Journal of Power Sources 196 (2011) 1847–1854

Contents lists available at ScienceDirect

Journal of Power Sources

journal homepage: www.elsevier.com/locate/jpowsour

Water transport characteristics in the gas diffusion media of proton exchange membrane fuel cell – Role of the microporous layer

Enju Nishiyama, Toshiaki Murahashi*

Department of Electric and Electronics Engineering, Fukui University of Technology, 3-6-1 Gakuen, Fukui 910-8505, Japan

ARTICLE INFO

Article history:
Received 13 July 2010
Received in revised form
17 September 2010
Accepted 21 September 2010
Available online 29 September 2010

Keywords:
Proton exchange membrane fuel cell
Gas diffusion media
Water transport
Water management
Capillary pressure
Microporous layer

ABSTRACT

Water transport through the gas diffusion media of a proton exchange membrane fuel cell (PEMFC) was investigated with a focus on the role of the microporous layer (MPL) coated on the cathode gas diffusion layer (GDL). The capillary pressure of the MPL and GDL, which plays a significant role in water transport, is derived as a function of liquid saturation using a pore size distribution (PSD) model. PSD functions are derived with parameters that are determined by fitting to the measured total PSD data. Computed relations between capillary pressure and liquid saturation for a GDL and a double-layered GDL (GDL + MPL) show good agreement with the experimental data and proposed empirical functions. To investigate the role of the MPL, the relationship between the water withdrawal pressure and liquid saturation are derived for a double-layered GDL. Water transport rates and cell voltages were obtained for various feed gas humidity using a two-dimensional cell model, and are compared with the experimental results. The calculated results for the net drag with application of the capillary pressure derived from the PSD model show good agreement with the experimental values. Furthermore, the results show that the effect of the MPL on the cell output voltage is significant in the range of high humidity operation.

1. Introduction

The proton exchange membrane fuel cell (PEMFC) has attracted a great deal of attention in the last decade as a promising high-efficiency low-emission power source for both mobile and stationary applications. However, there are still many problematic issues that must be overcome for this technology to be efficient and practical. One major problem is water management, which requires careful attention during operation of a state-of-the-art PEMFC. At low humidity, the proton exchange membrane and electrode assembly (MEA) lose water, which leads to a rapid increase in ohmic resistance. Conversely, if too much liquid water is present in the cell, then the pores in the electrodes are filled with water and the passage of reactant gases becomes obstructed. Therefore, the cell operation conditions and MEA components have to be well matched in order to avoid membrane dehydration and cathode flooding. In addition to experimental approaches, water management models are useful to achieve understanding of the processes that govern water transport to assist optimization of the fuel cell operating conditions and relevant electrode structures.

Water is generated in a PEMFC at the cathode, in addition to which, water is transported from the anode to the cathode by electro-osmotic drag. As water builds up at the cathode, back diffusion occurs. Water is transported from the cathode back to the anode, because the concentration of water, i.e. the activity, is higher at the cathode than that at the anode. The total water flux occurs by diffusion through the gas diffusion media. If the vapor pressure reaches saturation pressure, then the condensed vapor moves as a liquid. In such a case, multiphase flow is the transport mechanism for water flux. Permeability of a porous medium is one of the controlling factors that affect the rate at which fluids travels through pores. Any local blockage of usually open pores restricts reactant flow to the reaction sites, a phenomenon referred to as flooding. Flow of the liquid water in a porous medium is driven by capillary action generated by the liquid saturation gradients.

Capillary pressure increases as the pore radius decreases; therefore, it is important to determine the exact pore size distribution of the porous media and its hydrophobic or hydrophilic character. These parameters are usually obtained experimentally and are highly dependent on the material. Various measurements of capillary pressure have been reported [1–6]. Kumbur et al. presented a modified Leverett function to estimate the capillary pressure as a function of liquid saturation and hydrophobic additive content based on experimental data [1–3]. Carbon paper (SGL24BC, 24CC, and 24DC) and carbon cloth (ELAT1200) were employed as gas diffusion layers (GDLs) and were coated on one side with a microporous layer (MPL). Fairweather et al. conducted experimental measurements of capillary pressure for several GDLs (Toray TGP-090 and Avcarb P75T) after hydrophobic treatment and reported a significant hysteresis between the liquid intrusion and gas intru-

* Corresponding author. Tel.: +81 776292549; fax: +81 776297891.
E-mail address: murahasi@fukui-ut.ac.jp (T. Murahashi).

0378-7753/$ – see front matter © 2010 Elsevier B.V. All rights reserved.
doi:10.1016/j.jpowsour.2010.09.055

Nomenclature

List of symbols

a_j	activity of water in stream j (anode, cathode)
C_j	concentration of water in the membrane, mol cm^{-3}
D_w	diffusion coefficient of water, cm^2 s^{-1}
E_n	Nernst loss, V
$f_{r,k}$	fraction of pore size distribution, k
f_{HI}	fraction of hydrophilic component
F	Faraday constant, 96,485 C mol^{-1}
I	local current density, A cm^{-2}
$i_{o,j}$	exchange current density, A cm^{-2}
k	permeability of water, m^2
krh	relative permeability of water
M_{H_2O}	molar weight of water
n_d	electro-osmotic drag coefficient
N_{H_2O}	molar flux of water (perpendicular to the gas diffusion media), mol s^{-1} cm^{-2}
p	pressure, kPa
p_c	capillary pressure, kPa
R	gas constant, 8.314 J mol^{-1} K^{-1}
RH	relative humidity
r	pore radius
$r_{0,k}$	characteristic pore radius of pore size distribution, k
s_k	spread of pore size distribution, k
sl	liquid saturation
t_d	condensation temperature, °C
T	temperature, K
V	cell output voltage, V
V_{oc}	open circuit voltage, V
$v(r)$	normalized volume of pore
v_p	pore volume of porous media
x	coordinate along the gas channel
y	coordinate perpendicular to the gas diffusion media

Greek symbols

α	net drag of water per proton
β_κ	coefficient used in Eqs. (6) and (7); 1 for HI pores and −1 for HO pores
γ	surface tension, N m^{-1}
δ	thickness, cm
ε	porosity of the gas diffusion media
η	overpotential, V
θ_c	water contact angle
λ	water content in the membrane
τ	tortuosity factor
ξ	stoichiometry
σ	conductivity, Ω^{-1} cm^{-1}
ν	viscosity, Pa s

Subscripts

a	anode
c	cathode
HI	hydrophilic
HO	hydrophobic
k	component of pore size distribution
l	liquid
nw	non-wetting
sat	saturation
$total$	total
v	vapor

sion curves [5]. Gostick et al. also reported hysteresis characteristics in capillary pressure measurements for several GDLs (Toray TGP-090 and SGL10BA) [6].

Weber et al. have developed a model to calculate relevant parameters, such as liquid saturation, permeability and the average Knudsen radius, from capillary pressure measurements and structural properties such as the pore-size distribution and water contact angle [7].

There have been several reports regarding the effect of a MPL on a GDL [7–11]. Weber et al. insisted that a MPL enhances fuel cell performance, due to an increase of the liquid penetration depth into the membrane by the increased pressure [7,8]. Pasaogullari and Wang modeled the two-phase (water vapor and liquid water) flow and transport in the air cathode of a PEMFC and concluded that capillary action is a dominant transport process to remove water inside the two-phase zone [9]. Karan et al. reported that there was no statistically significant difference in the experimental net drag for cells with MPLs compared those without MPLs [10,11].

In this work, we present a method for computing the capillary pressure of both MPL and GDL as a function of liquid saturation using the pore size distribution (PSD) model. The model derives PSD functions of which the parameters are determined by fitting to the measured total PSD data. The second aim is to investigate the role of the MPL and the effect of capillary pressure on water transport and cell performance based on the PSD model. The computation results are compared with experimental water transport data.

2. Water transport characteristics by the PSD model

2.1. PSD model

Water transport mechanisms in gas diffusion media and catalyst layers are closely dependent on the pore size distribution (PSD) of the media/layer. Gas diffusion media are composite structures that exhibit either hydrophilic or hydrophobic properties, or both. The water contact angle (θ_c) for composite media is expressed as follows:

$$\theta_c = \cos^{-1}(f_{HI} * \cos\theta_{HI} + (1 - f_{HI}) * \cos\theta_{HO}), \quad (1)$$

where f_{HI} is the fraction of hydrophobic characteristic, and θ_{HI} and θ_{HO} are the water contact angles of the hydrophilic and hydrophobic components, respectively. Scanning electron microscopy (SEM) images of gas diffusion media show that pores coated with polytetrafluoroethylene (PTFE) consist of both a larger hydrophobic portion and a smaller hydrophilic portion. It has been reported that the fraction of hydrophobic pores in bare carbon paper ranges between 2% (SGL10BA) and 15% (TGPH 120) [12]. Therefore, it is assumed that the water contact angle of a hydrophobic pore is approximated by the combination of a 90% hydrophobic component and a 10% hydrophilic component using Eq. (1). On the contrary, a hydrophilic pore is approximated by the combination of a 10% hydrophobic component and a 90% hydrophilic component. We have assumed contact angles for bare carbon fiber and PTFE of 80° and 110°, respectively [7,13]. Surfacial contact angles of hydrophobic and hydrophilic pores were calculated using Eq. (1) as 83° and 107°, respectively, which were in agreement with the measured contact angles for bare and hydrophobic-treated carbon papers [13].

The PSD of the gas diffusion media is expressed by the summation of log normal distributions originally described by Weber et al. [7],

$$v(r) = \sum_k f_{r,k} \left\{ \frac{1}{r s_k \sqrt{2\pi}} \exp\left[-\frac{1}{2} \left(\frac{\ln r - \ln r_{0,k}}{s_k \sqrt{2}} \right)^2 \right] \right\}, \quad (2)$$

Table 1
Integration limits of the PSD model and coefficients in Eqs. (6) and (7).

	Pores filled with water	Integration limits	Coefficient in Eqs. (6) and (7)
Hydrophilic (HI)			
$p_c \le 0$	$r \le r_{c,HI}$	0 to $r_{c,HI}$	$\beta = 1$
$p_c > 0$	All pores	0 to ∞	
Hydrophobic (HO)			
$p_c < 0$	–	–	$\beta = -1$
$p_c \ge 0$	$r_{c,HO} \le r$	$r_{c,HO} \le \infty$	

where $v(r)$ is the normalized volume of pore radius r, $r_{o,k}$, and s_k are the characteristic pore radius and spread of distribution k, respectively. $f_{r,k}$ is the fraction of distribution k in the total distribution. These values are determined from fitting with the experimental PSD data. A pore of given radius r is determined as being either filled or empty at a capillary pressure p_c according to the corresponding pore radius r_c defined by Eq. (3),

$$r_c = -\frac{2\gamma \cos\theta_c}{p_c}. \tag{3}$$

Liquid saturation sl and relative liquid permeability krh, are important factors used to describe the two-phase transport in the gas diffusion media. sl is defined as the volume fraction of the volume occupied by the liquid phase $v_{p,l}$, divided by the total void volume of the porous media $v_{p,total}$,

$$sl = \frac{v_{p,l}}{v_{p,total}} = \frac{\int_{r_{c,1}}^{r_{c,2}} v(r)\,dr}{\int_0^{\infty} v(r)\,dr}. \tag{4}$$

krh is defined as the ratio of the effective liquid permeability through the pores occupied by the liquid phase k_l, to the permeability at complete saturation k_{sat}.

$$krh = \frac{k_l}{k_{sat}} = \frac{\int_{rc,1}^{r_{c,2}} r^2 v(r)\,dr}{\int_0^{\infty} r^2 v(r)\,dr}. \tag{5}$$

sl and krh can be calculated by integrating and summing for each region where liquid water is present using Eqs. (2), (4) and (5). The integration regions ($r_{c,1}$ to $r_{c,2}$) are different, depending on whether a pore is hydrophilic or hydrophobic and are shown in Table 1. The corresponding pore radii r_c at p_c are calculated from Eq. (3) and defined as $r_{c,HI}$ and $r_{c,HO}$ for hydrophilic and hydrophobic pores, respectively. Eqs. (6) and (7) are then derived:

$$sl = \sum_k \frac{f_{r,k}}{2}\left\{1 + \beta_k\, erf\left(\frac{\ln r_{c,h} - \ln r_{0,k}}{s_k\sqrt{2}}\right)\right\}, \tag{6}$$

$$krh = \sum_k \frac{f_{r,k}}{2}\left\{1 + \beta_k\, erf\left(\frac{\ln r_{c,h} - \ln r_{0,k}}{s_k\sqrt{2}} - s_k\sqrt{2}\right)\right\}, \tag{7}$$

where *erf* represents the error function. The coefficient β_k comes from the difference of integration limits and is defined as 1 for hydrophilic pores and −1 for hydrophobic pores.

2.2. Relation between the capillary pressure and liquid saturation

Several measured PSD curves have been reported for commercial carbon paper and cloth after hydrophobic treatment, usually with MPLs [1–3,12,14]. Kumbur et al. [1] measured hydrophilic and total PSD curves for carbon paper and cloth using the standard porosimetry technique developed by Porotech. We have applied the PSD function of Eq. (2) to the PSD curve measured for a double layered gas diffusion medium reported by Kumbur et al. (Fig. 3 in [1]). The total and hydrophilic PSD curves are well represented by two hydrophilic PSDs (HI1 and HI2) and four hydrophobic PSDs

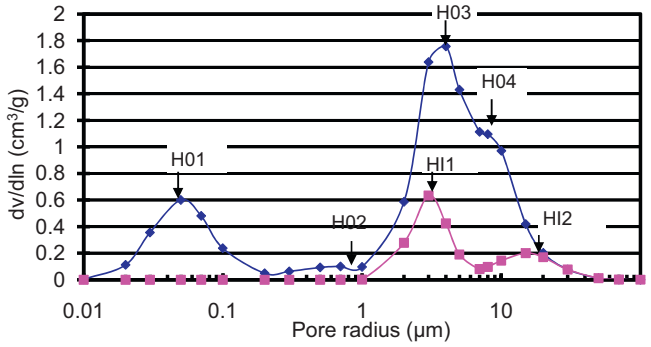

Fig. 1. Computed pore distribution for gas diffusion media. ♦: total pores; ■: hydrophilic pores.

(HO1–HO4), as shown in Fig. 1. The parameters of these PSDs are summarized in Table 2.

The relationship between capillary pressure and liquid saturation can be derived by applying Eqs. (3) and (6) to the PSD functions. The derivation process is as follows: firstly, a pressure is assumed and the liquid volume filled in six pore distributions are calculated and liquid saturation is derived by summation. The calculation is repeated assuming different pressures, and the results are shown in Fig. 2. Negative and positive capillary pressures correspond to hydrophilic and hydrophobic pores, respectively, and capillary pressure is zero at $sl = 0.222$. The capillary pressure varies stepwise in the curve, which reflects that the total PSD is composed of discrete PSDs. The capillary pressure for an HO1 micropore is out of the range of this figure, because the capillary pressure range is more than 100 kPa. This curve can be expressed approximately by a multi-power equation, which is represented as the solid line in Fig. 2:

$$P_c\ \text{(kPa)} = -75.723sl^5 + 440.53sl^4 - 495.54sl^3 + 161.14sl^2 + 24.358sl - 7.8799. \tag{8a}$$

Kumbur et al. proposed modified Leverett functions for a GDL with MPL to estimate the capillary pressure as a function of non-wetting liquid saturation and hydrophobic additive content for the hydrophobic pores [1]. The functions were approximated with the experimental capillary pressure data for carbon paper with PTFE contents ranging from 0 to 20 wt% and with the MPL. The calculated Eq. (8a) is comparable with these empirical functions. The modi-

Table 2
Structural properties of the gas diffusion media.

		GDL
Thickness	d	0.019
Hydrophobic contact angle	θ_{HO}	107
Hydrophilic contact angle	θ_{HI}	83
Porosity	e	0.8
Tortuosity factor	t	5
MPL		
Thickness	δ	0.005
Hydrophobic contact angle	θ_{HO}	107
Porosity	e	0.5

Pore size distribution characteristics

Pore k	Characteristic radius r_{ok}	Spread s_k	Fraction f_{rk}
HO1	0.05	0.25	0.21
HO2	1	0.5	0.04
HO3	4	0.15	0.36
HO4	9	0.1	0.18
HI1	3	0.1	0.14
HI2	15	0.2	0.07

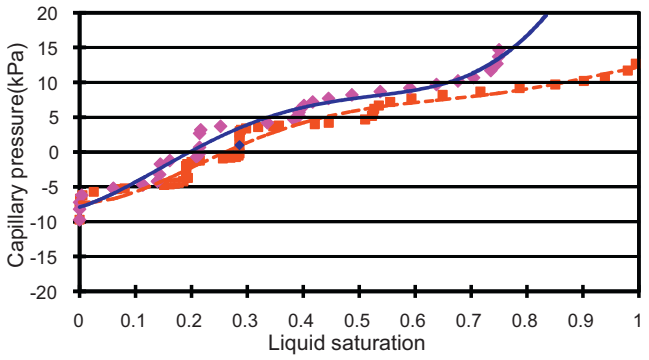

Fig. 2. Relation between capillary pressure and liquid saturation for gas diffusion media. ♦: estimation for a double-layered GDL, solid line is the approximation from Eq. (8a); ■: estimation for a GDL, dotted line is the approximation from Eq. (8b).

fied Leverett functions consist of three different expressions that correspond to the different liquid saturation regions: $0 \le sl_{nw} \le 0.5$, $0.5 \le sl_{nw} \le 0.65$, and $0.65 \le sl_{nw} \le 1$. The sl_{nw} values correspond to the hydrophobic region, so that it is necessary to transform $sl_{nw} = 0$ in the expression to $sl = 0.222$ from our calculation for comparison. The modified Leverett function (PTFE 5 wt%) is in good agreement with the results calculated from Eq. (8a) for $sl < 0.59$, as shown in Fig. 3a.

2.3. Pressure for water transport in gas diffusion media

2.3.1. Gas diffusion media (GDL and MPL)

A highly hydrophobic layer on a GDL is referred to as a MPL. A hydrophobic HO1 PSD (characteristics shown in Table 1) contributes the main part of the PSD for the MPL, as described by Kumbur et al. [1]. However, it is not clear whether the other hydrophobic PSD (HO2) belongs to either the GDL or MPL. SEM images indicate that the MPL is microporous with macro-cracks [13], which suggest that the MPL encompasses both hydrophobic HO1 and HO2 PSDs.

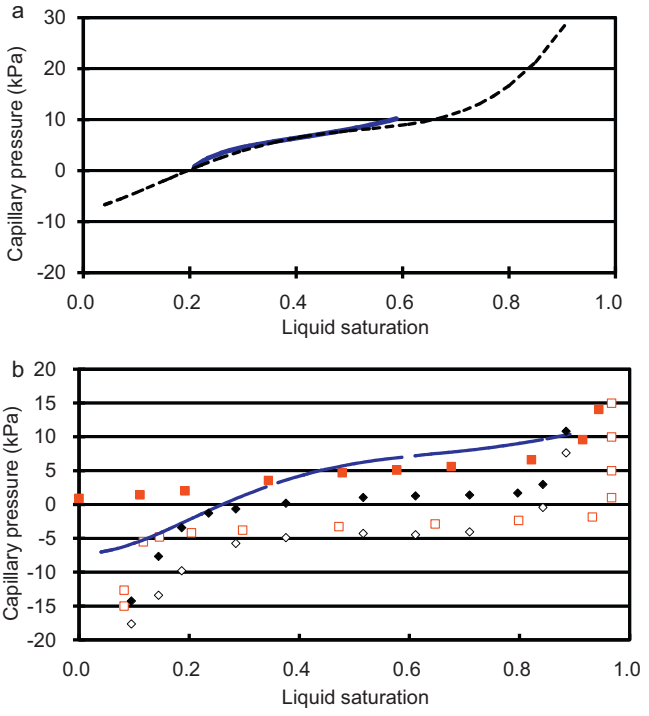

Fig. 3. (a) Comparison of the simulation results for capillary pressure as a function of liquid saturation using the modified Leverett function from Ref. [1]. The dotted line is the approximation from Eq. (8a) and the solid line is the modified Leverett function. (b) Comparison of the computed capillary pressure curves with experimental data. ♦, ◇: Fairweather et al. (♦: liquid intrusion, ◇: gas intrusion) [5]; ■,□: Gostick et al. (■: liquid intrusion, □: gas intrusion) [6]. The dotted line is the approximation from Eq. (8b).

The validity of the computed PSD characteristics for double-layered gas diffusion media (GDL + MPL) can be evaluated in terms of a comparison with the gas permeability. Assuming that Hagen-Poiseuille flow is applicable for porous media, then the relationship between permeability K and characteristic pore radius r, and the porosity ε is determined as [15]:

$$K = \frac{\varepsilon^3 r^2}{9(1-\varepsilon)^2 k_k}, \tag{9}$$

where k_k is the Kozeny constant, which represents the shape factor multiplied by the tortuosity factor. When a porous medium consists of several specific pores, then each permeability should be evaluated using Eq. (9) and summated. The following permeabilities are calculated for double-layered and bare GDLs, respectively, assuming that the pores are circular ($k_k = 2$ for circular pores) and applying the characteristic pore radius, fraction and porosity shown in Table 1: $K_{dGDL} = 0.121 \times 10^{-12}$ m^2 and $K_{GDL} = 3.74 \times 10^{-12}$ m^2. These values approximately coincide with the reported permeabilities for double layered and bare GDLs, $K_{dGDL} = 0.07$–0.58×10^{-12} m^2 and $K_{GDL} = 8.69$–31×10^{-12} m^2, respectively [14], which also suggests that the PSDs of the MPL consist of two types of PSD: HO1 and HO2.

The relationships between capillary pressure and liquid saturation for a GDL can be derived by applying Eqs. (3) and (6) to the PSD functions for HI1, HI2, HO3, and HO4 using the same process described in Section 2.2. These relationships can be expressed approximately by a multi-power equation as represented by the dotted line in Fig. 2:

$$P_c \ \text{(kPa)} = -204.37sl^5 + 604.99sl^4 - 625.82sl^3 + 249sl^2 - 4.4181sl - 7.1964. \tag{8b}$$

Several experimental data for p_c vs. sl reported by Fairweather et al. (Toray TGPH 090) [5] and Gostick et al. (SGL 10BA with 5% PTFE) [6] are also plotted in Fig. 3b for comparison with the calculated data. The capillary pressure calculated using Eq. (8b) shows negative values for $sl \le 0.2$ and increases gradually up to approximately 10 kPa at $sl \approx 0.8$. These characteristics are in agreement with the measured capillary pressure under conditions of water intrusion.

2.3.2. Relationship between the pressure for water transport and liquid saturation

The relationship between the pressure for water transport and liquid saturation for the GDL is derived using PSD functions for HI1, HI2, HO3 and HO4, and that for the MPL is derived using PSD functions for HO1 and HO2, and the results are shown in Fig. 4a and b, respectively. In Fig. 4a, the pressure data for hydrophilic pores are plotted as positive capillary pressures, because the necessary pressure for the withdrawal of liquid water from the porous media is positive. The relationships for a GDL are expressed approximately by the multi-power Eqs. (10a) and (10b), where sl_0 is the liquid saturation corresponding to zero capillary pressure. Pores corresponding to less than sl_0 are hydrophilic and are always filled with water under steady state operation.

In Fig. 4b, two curves are shown for the relationship between pressure for water withdrawal and liquid saturation. The curves pc–sl(a) and pc–sl(b) correspond to MPLs that consist of both hydrophobic HO1 and HO2 PSD, and only hydrophobic HO1 PSD, respectively. The capillary pressure of pc–sl(a) is much lower than that of pc–sl(b) in the low liquid saturation region, due to the presence of macro-cracks (HO2). Hereafter, we apply the pc–sl(a) curve

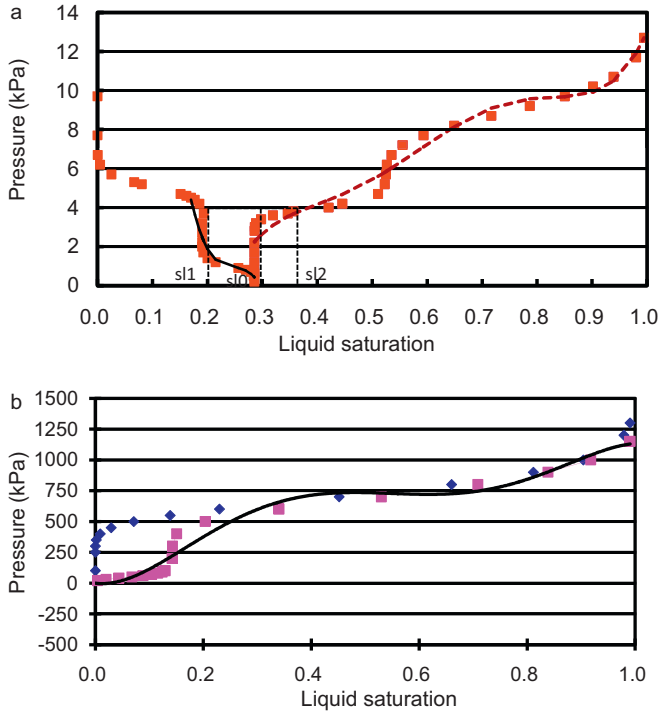

Fig. 4. (a) Pressure for water withdrawal from a GDL as a function of liquid saturation. ■: calculated pressure for water withdrawal. The dotted line represents the approximation from Eq. (10a), and the solid line represents the approximation from Eq. (10b). (b) Pressure for water transport through the MPL as a function of liquid saturation. ■: *pc–sl*(a), ♦: *pc–sl*(b). The solid line is the approximation from Eq. (10c).

as representative of a MPL. The relation for a MPL is approximated by Eq. (10c):

GDL:

$$P_{l,HO} = 1182.6sl^5 - 3585.4sl^4 + 4163.2sl^3 - 2311.1sl^2 + 627.62sl - 63.873, \quad sl \geq sl_0, \tag{10a}$$

$$P_{l,HI} = -6652.2sl^3 + 4950.3sl^2 - 1232.4sl + 103.58, \quad sl \leq sl_0, \tag{10b}$$

MPL:

$$P_l = -29,269sl^5 + 77,716sl^4 - 70,085sl^3 + 23,329sl^2 - 558.14sl. \tag{10c}$$

Almost the same relation is derived for the relative permeability constant *krh* and the capillary pressure P_l, i.e., the relationship $krh \cong sl$ exists.

2.4. Water transport by capillary pressure in gas diffusion media

The transport of liquid water from a cathode catalyst layer to the cathode flow channel is expressed as follows:

$$N_{H_2O,l} M_{H_2O} = \frac{krhS_e^2 K}{\nu} \nabla Pl, \tag{11}$$

where the relation $N_{H_2O,l} = I(1+2\alpha)/2F$ exists for the saturation condition and the relation $S_e^2 = (sl - sl0)^2$ is the correction factor, which reflects the separation and joining of liquid flow in gas diffusion media, as derived by Weber et al. [7]. The hypothesis is that transfer between liquid flow paths only occurs when the paths are of the same diameter. The right side term in Eq. (11) is the water flux of Darcy flow in the porous media, where $krhS_e^2K$ and ∇P_l are the relative permeability of water and the liquid pressure gradient in the GDL or MPL, respectively. The following relation is derived by integrating this equation in all regions of the porous media:

$$N_{H_2O,l} M_{H_2O} \frac{\nu}{K} \int_0^{\delta t} dy = \int_{sl_1}^{sl_2} krhS_e^2 \frac{dP_l}{dsl} dsl = \int_{sl_1}^{sl_0} krh(sl - sl_0)^2 \frac{dP_{l,HI}}{dsl} dsl + \int_{sl_0}^{sl_2} krh_0(sl - sl_0)^2 \frac{dP_{l,HO}}{dsl} dsl, \tag{12}$$

where δ is the thickness of the GDL or MPL, and sl_1 and sl_2 are the lower and upper limits of liquid saturation for liquid flow. Liquid saturation sl_1 belongs to the hydrophilic region and sl_2 belongs to the hydrophobic region, and $1 - sl_2$ is the gas diffusion space. There following relationship exists between sl_1 and sl_2,

$$P_{l,HI}(sl_1) = P_{l,HO}(sl_2). \tag{13}$$

$P_{l,HI}$ and $P_{l,HO}$ are multi-power functions of *sl*, so that by applying the approximate expression $krh = sl$. Eqs. (12) and (13) are expressed as multi-power functions of sl_1 and sl_2. These functions are solved by Newton method to obtain sl_1 and sl_2.

The presence of liquid water in gas diffusion media obstructs the diffusion of reactant gases. The diffusion space for cathode gas is reduced from 1 to the fraction $1 - sl_2$. The partial pressure drop of oxygen in the GDL becomes larger as the gas diffusion space is reduced, which causes an increase in the concentration polarization. *sl* at breakthrough indicates the threshold where the movement of accumulated liquid water through the GDL is initiated by a capillary pressure-controlled percolation process. The accumulation is the result of several effects, including the existence of the hydrophilic pores and the so-called ink-bottle effect. In the ink-bottle effect, as liquid enters a widening pore, the capillary forces change with the increasing diameter, which can trap a droplet [16]. Therefore, the liquid saturation at breakthrough corresponds to the diffusion space occupied by liquid water. Gostick et al. reported liquid saturation at breakthrough ranging between 0.14 and 0.20 for Toray 120C and 060C [17]. The value of 0.286 for sl_0 in our calculation (Fig. 4a) is almost the same as the reported liquid saturation at breakthrough.

Calculation of liquid saturation gives $sl_1 = 0.181$ and $sl_2 = 0.344$ for the GDL at the baseline operating condition shown in Table 2. The MPL consists of only hydrophobic pores; therefore, the relation $sl_0 = 0$ *always* exists. It is then possible to obtain sl_2 by solving only Eq. (12). A similar calculation for the MPL leads to $sl_2 = 0.056$. The change of the diffusion space as a function of the water flux was calculated using Eqs. (10a)–(10c) and (12), and is shown in Fig. 5. The relationship between *sl* and $N_{H_2O,l}$ shown in Fig. 5 is approximated by Eq. (14):

$$1 - sl_2 = 0.7143 - 231.25 N_{H_2O,l}^{0.6108}. \tag{14}$$

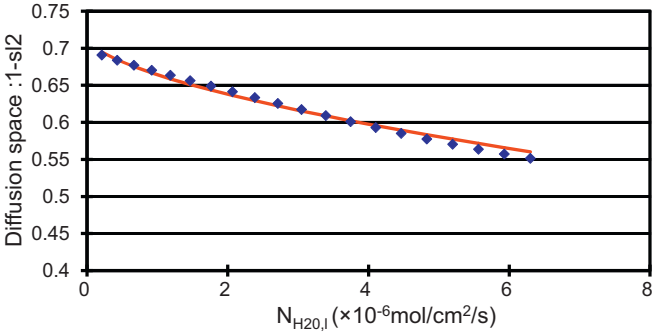

Fig. 5. Reduction of cathode reactant gas diffusion space as a function of water flux. The solid line is the approximation from Eq. (12).

The maximum water flux (6.3×10^{-6} mol cm^{-2} s^{-1} in Fig. 5) corresponds to a current density as large as 1.0 A cm^{-2}. The diffusion space decreases from 0.714 to 0.550 for this water flux range. The calculated partial pressure drop of oxygen in the GDL using the two-dimensional cell model (model formula are described in Section 3.1) is approximately 1% and the diffusion space is 0.645 under the baseline cell operation conditions. Therefore, a diffusion space of 0.550 at a current density of 1.0 A cm^{-2} suggests there is no significant increase in the concentration polarization.

3. The role of MPL in water transport from the anode to cathode

3.1. Cell model for simulation

The catalyst layer in the PEMFC is located between the membrane and gas diffusion media, and water is generated in this layer. There may be a pressure change in the catalyst layer when condensed liquid water moves to the membrane or cathode gas diffusion media. However, the pressure change in the catalyst layer is not significant compared with that of the MPL for the following reasons: (1) the short distances of water transport, and (2) larger hydraulic permeability [8]. Therefore, the pressure at the interface of catalyst layer/membrane is assumed to be the same as that at the catalyst layer/MPL interface. The pressure of the water at the cathode catalyst layer/membrane interface is higher than the saturation pressure, due to the presence of the hydrophobic MPL. Therefore, the activity of water at the cathode catalyst layer/membrane interface is increased when the vapor pressure reaches the saturation pressure. The pressure of water at the cathode catalyst layer/membrane interface is expressed by Eq. (15) with addition of the MPL capillary pressure $p_{c,MPL}$:

$$p = p_{sat} + p_{c,MPL}. \tag{15}$$

By applying Eq. (15) to the water activity at the cathode catalyst layer/membrane interface in a two-dimensional cell model [18,19], it is possible to calculate the net water drag α. The gas diffusion perpendicular to the MEA (y-direction) in this cell model is expressed by the Stefan-Maxwell equation under the condition of no nitrogen flux. The following relationships exist between the molar flux of oxygen, water and current density in the cathode along the flow channel (x-direction). In the model, the cell is divided into eight sections in the x direction.

$$N_{O_2} = -\frac{I(x)}{4F}, \tag{16}$$

$$N_{H_2O,c} = \frac{I(x)}{2F}(1 + 2\alpha). \tag{17}$$

Water is transported in the membrane by electro-osmotic drag caused by proton transport and back diffusion due to the activity (namely, concentration) gradient of water.

$$N_{H_2O,a} = n_d \frac{I(x)}{F} - D_w \frac{\partial C(x)}{\partial y} = \alpha \frac{I(x)}{F}. \tag{18}$$

The electro-osmotic drag coefficient n_d, diffusion coefficient D_w, and the water content in the membrane λ, are shown in Eqs. (19), (21) and (22), respectively.

$$n_d = 0.0049 + 2.024a_j - 4.53a_j^2 + 4.09a_j^3 = 1.59 + 0.159(a_j - 1), \tag{19}$$

$$a_j = C_j \frac{p}{p_{sat}}, \tag{20}$$

$$D_w = 1.1 \times 10^{-6} n_d \exp\left(2416\left(\frac{1}{303} - \frac{1}{T}\right)\right), \tag{21}$$

$$\lambda = 0.043 + 17.81a_j - 39.85a_j^2 + 36a_j^3. \tag{22}$$

The expressions given by Springer et al. for n_d, and λ are applied [20]. The expression for D_w is modified (the constant is twice as large as that of the previously reported value [19]), considering a recently reported Fickian diffusion coefficient that was experimentally obtained [21].

Eq. (23) shows the relationship between the cell output voltage V, cell overpotential η, and the ionic conductivity of the membrane σ.

$$V = V_{oc} - \frac{I(x)\delta_m}{\sigma} - (\eta_c + \eta_a) - E_n, \tag{23}$$

where V_{oc} and E_n are the open circuit voltage and Nernst loss, respectively. The cathode overpotential η_c, and anode overpotential η_a, are given using the exchange current densities i_{oc} and i_{oa}, respectively, as follows:

$$\eta_c = 1.5\frac{RT}{F}\ln\left(\frac{I(x)}{i_{oc}P_{O_2}}\right), \tag{24a}$$

$$\eta_a = 0.5\frac{RT}{F}\frac{I(x)}{i_{oa}P_{H_2}}. \tag{24b}$$

Based on the discussion in Section 2.4, another modification of the cell model has been made to consider the reduction of the gas diffusion space, expressed by Eq. (14). $N_{H_2O,l}(x)$ is calculated by determining the saturated water vapor from the water flux $N_{H_2O}(x)$ at each position along the flow channel.

3.2. Comparison of the model calculation and experimental net drag

3.2.1. Experimental

In this work, we present a method for computing the capillary pressure characteristics of a double layered GDL using the reported PSD data. We also investigate the role of the MPL and the effect of capillary pressure on the net drag using the derived capillary pressure characteristics and the calculated results are compared with that of the net drag measurement. A 25 cm^2 MEA was made of a Nafion 112 membrane, gas diffusion media of Toray carbon paper (TGH-090) treated with 10 wt% PTFE and a MPL which was made of carbon black and PTFE and was coated on one side of the GDL with the thickness of 30 μm. Net drag was derived through the measurement of the water condensed at the inlet and the exit of the test cell. Specification of the test cell and standard experimental condition are summarized in Table 3. Further details of the net drag measurement are described in the previous report [18].

3.2.2. Comparison of the calculation and experimental on the net drag

Although it is well known that properties of GDL depend on its venders, we apply the results on the capillary characteristics of a double layered GDL(SGL24DC) to the comparison of water transport characteristics from the following reasons: (1) Although there

Table 3
Specification of a test cell and standard test condition.

Membrane equivalent weight	1200
Membrane thickness (cm)	50×10^{-4}
Membrane dry density	1.84
Catalyst layer thickness (cm)	10×10^{-4}
GDL thickness (cm)	300×10^{-4}
Current density (A cm^{-2})	0.3
Cell temperature (°C)	80/70
Fuel	H_2
Cathode reactant gas	Air
Stoichiometry of anode gas, x_a	1.43
Stoichiometry of cathode gas, x_c	2
Pressure, kPa	101.3
Humidity of anode inlet gas, t_{da}	60

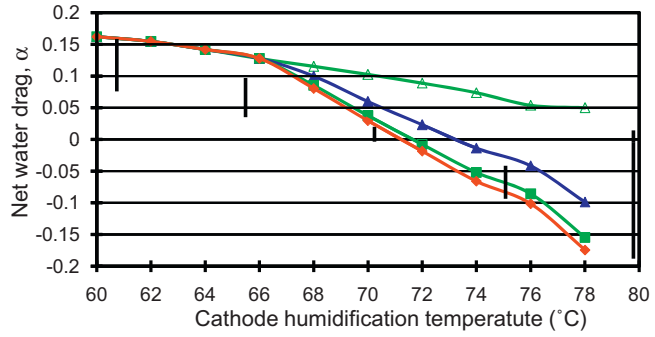

Fig. 6. Capillary effect on the net water drag α, as a function of the cathode humidification temperature. △: calculation without capillary effect; ▲, ♦, and ■: calculation with capillary effect (t_{cell} = 80 °C, t_{da} = 60 °C, ξ_f = 1.43, ξ_a = 2, ▲: $p_{c,MPL}$ = 12 kPa, ■: $p_{c,MPL}$ = 30 kPa, ♦: $p_{c,MPL}$ = 48 kPa). The solid vertical bars in the figure represent the experimental data distribution ranges.

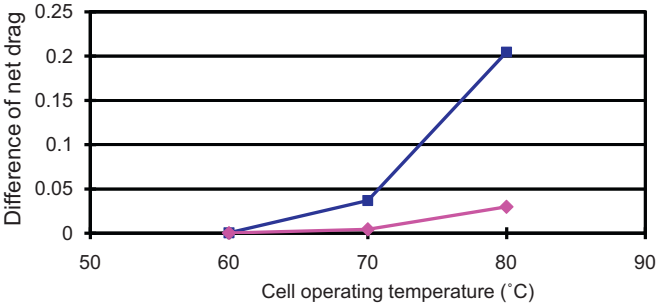

Fig. 7. Change in the capillary effect on the net drag α, as a function of the cell operation temperature and relative humidity (ξ_f = 1.43, ξ_a = 2, $p_{c,MPL}$ = 30 kPa). ■: high humidity condition (RH = 93–100%), ♦: low humidity condition (RH = 44–69%).

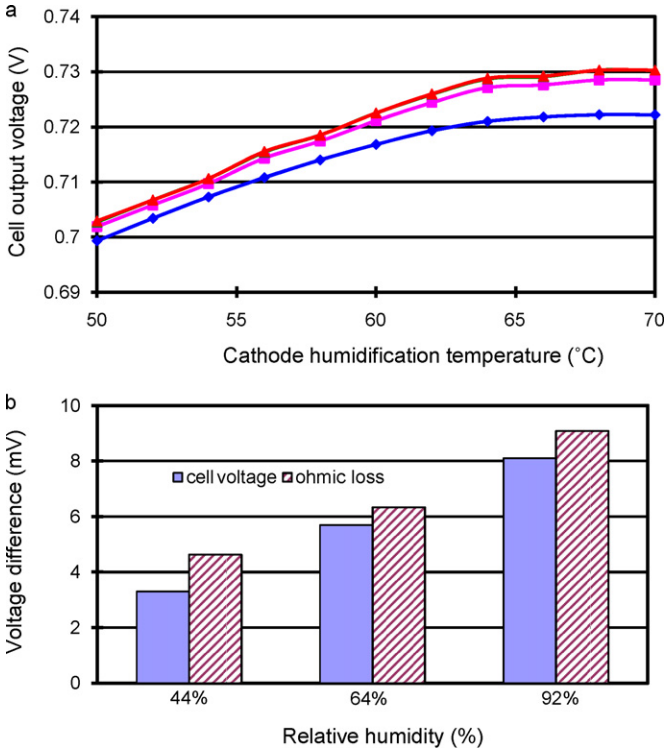

Fig. 8. (a) Effect of the MPL on cell performance as a function of the cathode humidification temperature (t_{cell} = 70 °C, t_{da} = 60 °C, ξ_f = 1.43, ξ_a = 2, ♦: $p_{c,MPL}$ = 0, ■: $p_{c,MPL}$ = 12 kPa, ●: $p_{c,MPL}$ = 30 kPa, ▲: $p_{c,MPL}$ = 48 kPa). (b) The differences in cell output voltage and ohmic loss in the membrane with and without the MPL at several cathode inlet humidities (t_{cell} = 70 °C, t_{da} = 60 °C, ξ_f = 1.43, ξ_a = 2, $p_{c,MPL}$ = 30 kPa).

exist some differences in the porosity, peak pore diameter and surface energy of these carbon papers [12,13], these differences do not exceed about 10% of the values. (2) For the calculation of capillary pressure characteristics, it is necessary to know both the hydrophilic and the total PSD of a GDL. The PSD data of SGL24DC by Kumbur et al. is the only available data which gives both hydrophilic and total PSD.

The net drag was calculated for varying capillary pressure p_c. The capillary pressure of the MPL, which corresponds to sl_2 = 0.056 (calculation process shown in Section 2.4) is 30 kPa. $p_{c,MPL}$ is varied from 12 to 48 kPa (a range of ±18 kPa was selected for both the upper and lower limits from the computed value of 30 kPa) and the results are shown in Fig. 6. There was no significant difference in the computed net water drag for all $p_{c,MPL}$ in the low humidity region (t_{dc} < 65 °C). However, as the inlet humidity increases, the net drag for $p_{c,MPL}$ = 30 and 48 kPa decreased abruptly, which is in good agreement with the experimental data and suggests that the hydrophobic micropores of a MPL act to transfer water from the cathode to anode and reduce the possibility of flooding in the cathode GDL.

Karan et al. claimed that the effect of the MPL does not significantly increase the water transport from the cathode to the anode, according to experimental data [10,11]. However, the effect of the MPL is prominent under high humidity conditions and the effect of the MPL on the net drag is dependent on the cell operation conditions. For example, calculated net drags for a GDL without MPL and a double-layered GDL ($p_{c,MPL}$ = 30 kPa) are shown in Fig. 7, and the cell operation conditions are the same as those listed in Table 3, except the cell operation temperature. The difference in the net drag is larger as the cell operation temperature is increased and as the humidity is increased.

4. Discussion

4.1. Role of the MPL for improvement of cell performance

The MPL has another role; the improvement of cell performance. When a cell is operated under relatively low humidity conditions, it is desirable to keep the MEA wet in order to reduce the membrane resistance. On the contrary, when a cell is operated in the saturated condition, generated water should be quickly removed from the reaction sites.

Cell performance was computed as a function of the cathode humidification temperature and the results are shown in Fig. 8a. The cell operation conditions are the same as those listed in Table 3, except for the humidification temperature of the cathode reactant gas. For all regions, the cell output voltage increased with the capillary pressure of the MPL. The cell performance was improved with both increases in the cathode humidification temperature and the capillary pressure, and the results suggest an optimum capillary pressure for the MPL in the range between 30 and 48 kPa.

The increase of the cell output voltage is mainly due to the conductivity reflected by the water content λ, in the membrane. The differences in cell output voltage and ohmic loss in the membrane with and without the MPL ($p_{c,MPL}$ = 30 kPa) at several cathode inlet humidities are shown in Fig. 8b. The increase in cell output voltage is almost equal to the decrease of ohmic loss of the membrane, except under low humidification, where the cathode overpotential increases significantly due to the local current density distribution along the flow channel.

4.2. Relationship of MPL and the catalyst layer structure

When the pressure of water transport from the MPL is higher than the capillary pressure of the hydrophobic pores in the catalyst layer, the water generated in the cell reaction may cause flooding in

the catalyst layer. Therefore, the optimum capillary pressure, i.e., the optimum PSD for the MPL, also depends on the PSD and its apparent water contact angle to the catalyst layer.

Uchida et al. reported that the PSD for the catalyst layer consists of primary pores (<0.04 μm) and secondary pores (0.04–1 μm), and the latter corresponds to the gas paths [22,23]. They also reported that the specific pore volume distribution of the best performance cell had an average pore radius of approximately 0.1 μm. The capillary pressure of the hydrophobic pores with a characteristic radius of 0.1 μm is approximately 425 kPa for a contact angle of $\theta_c = 110^\circ$. When the capillary pressure of the MPL (ranged from 12 to 48 kPa) is less than the capillary pressure of the catalyst layer, then flooding does not occur in the catalyst layer. However, more information is required with regard to the contact angle and pore size distribution in the catalyst layer to obtain a certain conclusion.

5. Conclusion

Water transport through the gas diffusion media of a PEMFC was investigated with a focus on the role of the MPL on the cathode GDL. The capillary pressures of the MPL and GDL were estimated using the PSD model. PSD functions are derived, of which the parameters are determined by fitting to the measured total PSD data. The capillary pressure calculated for a GDL with MPL was in good agreement with the experimental results at low liquid saturation. For a GDL without MPL, the calculated capillary pressure was also in good agreement with the measured capillary pressure under water intrusion.

Based on the relationships between capillary pressure and liquid saturation, mass balance equations along the cathode flow channel were solved to obtain water transport rates and cell voltages for various feed gas humidification. The capillary pressure of the MPL relates to the activity of water at the cathode catalyst layer/membrane interface and has the effect of decreasing the net water drag from the anode to the cathode. The net drag calculated from the PSD model with consideration of the capillary pressure corresponded well with the measured values.

The effect of the MPL capillary pressure on the cell output voltage was significant for cell operation under high humidity conditions, which suggests that the wetness of the MEA has an optimum pore size distribution and the contact angle of the catalyst layer to prevent flooding.

Acknowledgement

This work was supported by the Open Research Center Project from the Ministry of Education, Culture, Sports, Science and Technology of Japan.

References

[1] E.C. Kumbur, K.V. Sharp, M.M. Mench, J. Electrochem. Soc. 154 (2007) B1295–B1304.
[2] E.C. Kumbur, K.V. Sharp, M.M. Mench, J. Electrochem. Soc. 154 (2007) B1305–B1314.
[3] E.C. Kumbur, K.V. Sharp, M.M. Mench, J. Electrochem. Soc. 154 (2007) B1320–B1324.
[4] T.V. Nguyen, G. Lin, H. Ohn, X. Wang, Electrochem. Solid-State Lett. 11 (2008) B127–B131.
[5] J.D Fairweather, P. Cheng, J. St-Pierre, D.T. Schwarts, Electrochem. Commun. 9 (2007) 2340–2345.
[6] J.T. Gostick, M.A. Ioannidis, M.W. Fowler, M.D. Pritzker, Electrochem. Commun. 10 (2008) 1520–1523.
[7] A.Z. Weber, R.M. Daring, J. Newman, J. Electrochem. Soc. 151 (2004) A1715–A1727.
[8] A.Z. Weber, J. Newman, J. Electrochem. Soc. 152 (2005) A677–A688.
[9] U. Pasaogullari, C.Y. Wang, J. Electrochem. Soc. 151 (2004) A399–A406.
[10] H.K. Atiyeh, K. Karan, B. Peppley, A. Phoenix, E. Halliop, J. Pharoah, J. Power Sources 170 (2007) 111–121.
[11] K. Karan, H. Atiyeh, A. Phoenix, E. Halliop, J. Pharoah, Electrochem. Solid-State Lett. 10 (2007) B34–B38.
[12] M.V. Williams, E. Begg, L. Bonville, H.R. Kunz, J.M. Fenton, J. Electrochem. Soc. 151 (2004) A1173–A1180.
[13] D.L. Wood, C. Rulison, R.L. Borup, J. Electrochem. Soc. 157 (2010) B195–B206.
[14] M.J. Martinez, S. Shimpalee, J.W. Van Zee, A.V. Sakers, J. Electrochem. Soc. 156 (2009) B558–B564.
[15] B. Sunden, M. Faghri, Transport Phenomena in Fuel Cells, WIT Press, 2005, p. 182.
[16] M.W. Mench, Fuel Cell Engines, John Wiley & Sons, Inc., 2008, p. 261.
[17] J.T. Gostick, M.A. Ioannidis, M.D. Pritzker, M.W. Fowler, J. Electrochem. Soc. 157 (2010) B563–B571.
[18] T. Murahashi, M. Naiki, E. Nishiyama, J. Power Sources 162 (2006) 1130–1136.
[19] T. Murahashi, H. Kobayashi, E. Nishiyama, J. Power Sources 175 (2008) 98–105.
[20] T.E. Springer, T.A. Zawodzinski, S.W. Gottesfeld, in: R.E. White, M.W. Verbrugge, J.F. Stockel (Eds.), Modeling Water Content Effects in Polymer Electrolyte Fuel Cells, PV91-10, Electrochemical Society Softbound Series, 1991, p. 209.
[21] S. Motupally, A.J. Becker, J.W. Weidner, J. Electrochem. Soc. 147 (2000) 3171–3177.
[22] M. Uchida, Y. Fukuoka, Y. Sugawara, N. Eda, A. Ohta, J. Electrochem. Soc. 143 (1996) 2245–2252.
[23] M. Uchida, Y. Fukuoka, Y. Sugawara, N. Eda, A. Ohta, J. Electrochem. Soc. 145 (1998) 3708–3713.